

1 **Test**

2 **Alexander Beck¹, Jan Henneberger¹, and Ulrike Lohmann¹**

3 ¹Institute for Atmospheric and Climate Sciences, ETH Zurich, Zurich, Switzerland

4 **Key Points:**

- 5 • In-situ measurements of microphysical cloud properties with a holographic Imager
6 • Influence of in-situ cloud observations at mountain top stations by ground based ice
7 enhancement processes
8 •

9 **Abstract**

10 In-situ cloud observations at mountain-top research station regularly measure ice crystal
 11 number concentrations (ICNCs) orders of magnitudes higher than expected from mea-
 12 surements or simulations of ice nuclei particle concentrations. Several studies suggest
 13 mountain-top in-situ measurements are influenced by surface-based ice-enhancement pro-
 14 cess, e.g. blowing snow, hoar frost or riming on snow covered trees, rocks and the remain-
 15 ing snow surface. A strong influence of in-situ observations on mountain-top stations by
 16 surface-based ice-enhancement processes may limit relevance of such measurements and
 17 could have an impact on orographic clouds.

18 This study assesses the influence of surface-based ice-enhancement processes on
 19 in-situ cloud observations at the Sonnblick Observatory in the Hohen Tauern Region,
 20 Austria. Vertical profiles of ICNCc above a snow covered surface were observed up to a
 21 height of 10 m. In clouds, the ICNCs decreased by at least a factor of two in the observed
 22 height interval. During a cloud-free period the ICNC decreases from several hundreds per
 23 liter near the ground to 10 per liter at a height of 10 m.

24 Information on wind, spectra and habit...

25 For one case study a correlation between ICNC and horizontal wind speed was ob-
 26 served for wind speeds below 10 m s^{-1} . for wind , a dependency of the ICNC on the hor-
 27 izontal and vertical wind speed was observed. These observations strongly suggest that
 28 mountain-top in-situ measurements are strongly influenced by surface-based ice-enhancement
 29 processes.

30 **1 Introduction**

31 The microphysical properties (e.g. phase composition, cloud particle number con-
 32 centrations) and cloud processes are key parameters for the clouds lifetime, the cloud ex-
 33 tent, as well as the intensity of precipitation they produce [Rotunno and Houze, 2007]. For
 34 example, the phase composition influence the radiative properties of midlevel clouds in
 35 the temperature range between 0 to -35 °C. A pure ice cloud in this temperature regime
 36 reflects 17 W m^{-2} more radiation than an pure liquid cloud [Lohmann, 2002]. A well rep-
 37 resentation of orographic mixed-phase clouds is therefore crucial for accurate weather pre-
 38 dictions in alpine terrain and improved climate models.

39 In-situ measurements are important to improve our understanding of microphysical
 40 properties and fundamental processes of orographic mixed-phase clouds [Baumgardner
 41 et al., 2011] and are frequently conducted at mountain-top research stations. Despite an
 42 improved understanding on the origin of ice crystals from nucleation (citation!!!!) as well
 43 as from secondary ice-multiplication processes [Field et al., 2017], the source of most of
 44 the ice crystals observed at mountain-top stations and their impact on the development of
 45 the cloud remains an enigma (citation!!!!).

46 In-situ observations with aircraft usually observe and ICNC on the order of $1\text{-}101^{-1}$
 47 [Gultepe et al., 2001], whereas at mountain-top research stations (e.g. Elk Mountain, USA
 48 or Jungfraujoch, Switzerland) or near the snow surface in the Arctic ICNCs of several
 49 hundreds to thousands per liter are frequently reported [Rogers and Vali, 1987; Lachlan-
 50 Cope et al., 2001; Lloyd et al., 2015]. Secondary ice multiplication processes like frag-
 51 mentation [Rangno and Hobbs, 2001] or the Hallett-Mossop process [Hallet and Mossop,
 52 1974] are usually ruled out as the source for the observed ice crystals due to the lack of
 53 large ice crystals, respectively large cloud droplets or the wrong temperature range. In-
 54 stead surface-based ice-enhancement processes are proposed to produce such enormous
 55 ICNCs. Rogers and Vali [1987] suggested two possible processes as a source for the ob-
 56 served ICNC: riming on trees, rocks and the snow surface or the lifting of snow particles
 57 from the surface, i.e. blowing snow. In addition, Lloyd et al. [2015] suggested hoar frost

as a wind independent, surface-based ice-enhancement process to cause ICNCs larger than 100 l^{-1} for which they didn't observe a wind dependency as expected for blowing snow. Although different studies are strife about the mechanisms to explain the measured high ICNCs, they agree on an strong influence by surface-based processes.

While the influence of mountain-top measurements by surface-based processes is widely accepted, the impact of re-suspended ice crystals on the development of super-cooled orographic clouds, e.g. a more rapid glaciation and enhanced precipitation, has not been studied extensively [Geerts *et al.*, 2015]. If the proposed surface-based ice-enhancement processes have the potential to impact the development of a cloud depends primarily on the penetration depth of the reseuspended particle into a cloud, i.e. the maximum height above the surface to which the particles get lifted.

The height dependency of blowing snow has been studied in the context of snow redistribution ("snow drift") and reduced visibility due to the re-suspended ice crystals by observing ice crystals up to several meters above the snow surface [Schmidt, 1982; Nishimura and Nemoto, 2005]. It has been reported that blowing snow occurs above a wind speed threshold that varies between 4 m s^{-1} and 13 m s^{-1} [Bromwich, 1988; Li and Pomeroy, 1997; Mahesh *et al.*, 2003; Déry and Yau, 1999]. Besides the wind speed, the concentration of blowing snow depends on the snowpack properties () and on the atmospheric conditions (current temperature, humidity) [Vionnet *et al.*, 2013]. Nishimura and Nemoto [2005] observed the ICNC up to a height of 9.6 m and found that the ICNCs usually decrease to as low as 1-10 particles per liter. During a precipitation event, the relative importance of the small ice crystals below $< 100\text{ }\mu\text{m}$ decreases from nearly 100 % at 1.1 m to below 20 % at 9.6 m. The rapid decrease of ICNCs with height observed by these studies may limit the impact of blowing snow on orographic clouds. However, most of these studies were conducted in dry air conditions where ice crystals undergo rapid sublimation [Yang and Yau, 2008], which may limit the applicability of these results.

Lloyd et al. [2015] suggested that vapor grown ice crystals on the crystalline surface of the snow cover, i.e. hoar frost, may be detached by mechanical fracturing due to turbulence independent of wind speed. To our knowledge only one modelling study exists, which asses the impact of haor frost on the development of a cloud. *Farrington et al.* [2015] implemented a flux of surface hoar crystals in the WRF (Weather Research and Forecasting) model based on a frost flower aerosol flux to simulate ICNCs measured at the Jungfraujoch by *Lloyd et al.* [2015]. They concluded, that the surface-based ice-crystals have a limiting impact on orographic clouds because the ice crystals are not advected high into the atmosphere. However, more measurements of ice-crystal fluxes from the snow covered surface are necessary to simulate the impact of surface-based ice-crystal enhancement processes on the development of orographic clouds [*Farrington et al.*, 2015].

In contrast to these finding, several remote sensing (i.e. satellite, lidar and radar) studies measured ice crystals advected as high as 1 km above the surface, which suggest an impact of surface-originated ice-crystals on clouds. Satellite observations of blowing snow from MODIS and CALIOP over the Antarctica [Palm *et al.*, 2011] observed layer thickness up to 1 km with an average thickness of 120 m for all observed blowing snow events. Similar observations from lidar measurements exist from the South Pole with an observed layer thickness of ice crystals of usually less than 400 m, but some rare cases when a subvisual layer exceeded a height of 1 km [Mahesh *et al.*, 2003]. However, a possible suspension of clear-sky precipitation could not be ruled out as a source of the observed ice crystal layers. Observations of layers of ice crystals from radar measurements on an aircraft in the vicinity of the Medicine Bow Mountains [Vali *et al.*, 2012] observed ground-layer snow clouds which where most of the time not visually detectable but produced a radar signal. Resuspended ice crystals from the surface or riming of cloud droplets at the surface can be the origin of the ice crystals in such ground-layer snow clouds. *Geerts et al.* [2015] presented evidence for ice crystals becoming lofted up to 250 m in the atmosphere by boundary layer separation behind terrain crests and by hy-

draulic jumps. Also evidence that ice crystals from the surface may lead to the glaciation of supercooled orographic clouds and enhanced precipitation were found. However, *Geerts et al.* [2015] also mention the limitation of radar and lidar measurement to separate the small ice crystals produced by surface processes from the larger falling snow particles and more abundant cloud droplets. They even concluded, that "to explore BIP (blowing snow ice particle) lofting into orographic clouds, ice particle imaging devices need to be installed on a tall tower, or on a very steep mountain like the Jungfraujoch".

In this study we assess the influence of surface-based ice-enhancement processes on in-situ cloud observations at mountain-top stations and the a potential impact on orographic mixed-phase clouds. Therefore, vertical profiles of the ICNC up to a height of 10 m above the surface are observed for the first time in cloud at the Sonnblick Observatory. Ice crystals are recorded with the holographic imager HOLIMO, capable of observing ice crystals larger than 25 μm [*Beck et al.*, 2017].

2 Field Measurements at the Sonnblick Observatory

2.1 Site description

This field campaign was conducted at the Sonnblick Observatory (SBO) situated at the summit of Mt. Sonnblick at 3106 masl ($12^{\circ}57'\text{E}$, $47^{\circ}3'\text{N}$) in the Hohen Tauern National Park in the Austrian Alps. The SBO is a meteorological observatory operated all year by the ZAMG (Central Institute for Meteorology and Geodynamics). On the East and South the SBO is surrounded by large glacier fields with a moderate slope, whereas on the Northeast a steep wall of approximately 800 m descends to the valley (Fig. 1, right). Part of the SBO is a 15 m high tower used for meteorological measurements by the ZAMG. The data presented in this paper was collected during a field campaign in February 2017.

2.2 Instrumentation

The microphysical properties of clouds, hydrometeors and resuspended particles from the surface were observed with the holographic Imager HOLIMO, which is part of the HoloGondel platform [*Beck et al.*, 2017]. The holographic Imager was mounted on an elevator that was attached to the meteorological tower of the SBO (Fig. 2) to obtain vertical profiles of the microphysical properties up to a height of 10 m above the surface where the platform was repeatedly positioned at five different heights as indicated in Figure 2. The holographic imager HOLIMO had a distance of approximately 1.5 m from the tower on the east-northeast side of the tower (Fig. 1, right). The holographic imager HOLIMO captures the information of cloud particles in a three-dimensional volume on a single image. In this study a sample volume of 16 cm^3 with a length of 6 cm along the optical axis was examined. The data is averaged over 50 holograms and a total volume of 800 cm. The open source software HoloSuite [*Fugal*, 2017] is used to reconstruct the in-focus images of the particles. Particles smaller than 25 μm are classified as liquid droplets, whereas particles larger than 25 μm are separated in liquid droplets and ice crystals based on the shape of their 2D image. Similar to a study by *Schlenzeck and Fugal* [2017] the ice crystals were further visually classified into three different groups: regular, irregular and aggregates. Because the visual classification of several thousands of ice crystals is time consuming this sub-classification of ice crystals was done only for the profiles on February 17th.

Meteorological data are available from the measurements by the ZAMG and the HoloGondel platform. The ZAMG measures one minute averages of temperature, relative humidity and horizontal wind speed and direction at the top of the meteorological tower. Snow cover depth is daily manually observed by the operators of the SBO. Based on these measurements the change of the snow cover is calculated. However, this calculation includes all the changes in the snow cover depth, e.g. snow drift, sublimation, melting

160 and fresh snow. Daily measurements of the total precipitation are available on the North
 161 and South side of the SBO. A ceilometer located in the valley on the North of the SBO
 162 measured the cloud base and cloud depth. An additional 3D Sonic Anemometer, which is
 163 part of the HoloGondel platform [Beck *et al.*, 2017], was mounted at the top of the meteo-
 164 rological tower. However, data is only available occasionally, because most of the time the
 165 heating of the Anemometer was not sufficient enough to prevent the build up of rime on
 166 the measurement arms.

167 3 Results

168 The data presented were observed on 4 February and 17 February 2017. Figure 3
 169 and 4 show an overview on the meteorological conditions on both days. The main differ-
 170 ence is the wind direction, which was South-West on 4 February and North on 17 Febru-
 171 ary.

172 3.1 4 February 2017

173 On 4 February a low pressure system moved eastwards from the Atlantic Ocean over
 174 northern France to western Germany, where it slowly dissipated. Influenced by this low
 175 pressure system the wind at the SBO predominantly came from West-Southwest and wind
 176 speeds between 10 and 25 m s⁻¹. In the late afternoon around 1900 UTC, when the low
 177 pressure system dissipated over western Germany, the wind direction changed to North
 178 and wind speeds decreased to a minimum of 5 m s⁻¹. After 1900 UTC wind speed in-
 179 creased again to up to 15 m s⁻¹. Starting from 0800 UTC the SBO was in cloud except
 180 for a short time interval between 1910 and 2020 UTC. The temperature didn't change
 181 much during the day and stayed between -10 and -9 °C until 1900 UTC when the wind
 182 direction changed to North and the temperature decreased to -11 °C at 22 UTC.

183 Between 0830 and 2200 UTC, a total of 24 vertical profiles were obtained. Because
 184 no data is available from the 3D Sonic Anenometer, only one minute averages of tem-
 185 perature, wind speed and direction are available from the ZAMG measurements (Fig. 3).
 186 Most of the profiles were obtained when the station was in cloud expect for four profiles
 187 between 1910 and 2020 UTC as indicated in Figure 3. The ICNC as a function of height
 188 summarized over 24 vertical profiles obtained on 4 February is shown in Figure 5. The
 189 ICNC reaches a maximum at 2.5 m above the surface. Compared to this maximum, the
 190 mean ICNC at a height of 10 m decreases by a factor of two and the median ICNC even by
 191 a factor of four. These observations suggest an influence of the measurements close to the
 192 snow surface by surface based ice crystal enhancement processes and a rapid decrease of
 193 the ICNC with height.

194 Figure 6 shows four time periods representing different conditions during the 4 Febru-
 195 ary. For the vertical profiles obtained between 1910 and 2010 UTC (Fig. 6 first row),
 196 when the SOB was not in cloud, the ICNCs have their maximum at a height of 2.5 m.
 197 The maximum ICNC at this height reaches up to 600 l⁻¹. For three of the profiles, the
 198 ICNC decrease by more than a factor of 5 from over 100 l⁻¹ at 2.5 m to less than 20 l⁻¹ at
 199 10 m. The mean ICNC decreases from around 100 l⁻¹ at 2.5 m to 10 l⁻¹ at 10 m (Fig. 6,
 200 right panel in the first row). The large extend of the shaded area at 2.5 m represents the
 201 high variability of the ICNC even when the data is averaged over 50 holograms. Because
 202 the SBO was not in cloud during this time period, these measurements strongly suggest an
 203 influence by surface based processes at a wind speed of less than 10 m s⁻¹ of up to several
 204 hundreds of ice crystals per liter at a height of 2.5 m.

205 Between 2030 and 2200 UTC (Fig. 6 second row), when the SBO was in cloud
 206 again, the vertical profiles of the ICNC show a similar tendency as in the cloud free pe-
 207 riod. The maximum of the ICNC was observed at a height of 4.1 m and the ICNC de-
 208 creases consistently for all four profiles with height above the observed maximum. The

209 boxplot on the right of Figure 6 shows that the mean of the ICNC decreases by a factor
 210 of 9 from its maximum at 4.1 m to its minimum at 10 m. This decrease is in the same or-
 211 der of magnitude as in the cloud free case discussed above. Assuming that the observed
 212 ICNC at 10 m is representative for the cloud without surface influence, the surface-based
 213 processes contribute with several hundreds of ice crystals per liter to the measurements at
 214 2.5, 4.1 and 6.0 m. This surface-based contribution is in the same order of magnitude as
 215 the total measured ICNCs in the cloud free period observed between 1910 and 2020 UTC.
 216 The influence extends to a height of 6.0 m, which is probably due to an increased wind
 217 speed of up to 15 m s^{-1} .

218 The highest ICNCs were observed in the time period between 1200 and 1500 UTC
 219 (Fig. 6 second row) when also the wind speed reaches its maximum of 25 m s^{-1} . The box-
 220 plot for this time interval shows a maximum ICNC at 2.5 m in the range of 500 to 900 l^{-1}
 221 and a decrease by a factor of 2 within 7.5 m. This decrease is much lower than observed
 222 in the previous time interval and is most likely due to the high wind speeds. Between dif-
 223 feren profiles the ICNC changed by a factor of, however, the trend of a decreasing ICNC
 224 with height was observed consistently for all profiles.

225 In the morning between 0830 and 1100 UTC the observed ICNCs (Fig. 6 first row)
 226 are much lower than between 1200 and 1500 UTC, although wind speed was as high as
 227 20 m s^{-1} . A possible reason is the history of the snowpack before 04 February 2017. The
 228 last snow fall was observed on ?? February 2017 and most of the loose ice crystals on top
 229 of the snowpack possibly already have been blown away. Therefore, higher wind speeds are
 230 necessary to resuspend ice crystals from the snowpack.

231 To get an estimate of the correlation between wind speed and ICNC, the ICNC
 232 is averaged over a time interval of 1 min and compared to the maximum wind speed in
 233 the corresponding 1 min time interval observed by the SBO on top of the meteorological
 234 tower. Maximum wind speed is used rather the average wind speed, because it is expected
 235 that the gusts, i.e. the highest wind speed in an time interval are most relevant for resus-
 236 pending ice crystals from the surface. For the time interval between 0830 an 1500 UTC
 237 when the wind direction was west-southwest (Fig 7, top) the ICNC shows no strong cor-
 238 relation is observed for wind speeds higher than 14 m s^{-1} . For the time interval bwetween
 239 1910 and 2230 UTC (Fig 7, bottom), when the wind direction was north, a much more
 240 pronounced dependency of the ICNC on wind speed is observed for wind speeds lower
 241 than 14 m s^{-1} . This is a possible indication that the ice crystal concentration reaches a sat-
 242 uration for wind speed larger than 14 m s^{-1} for the conditions on 04 February 2014.

243 3.2 17 February 2017

244 On 17 February a cold front over northern Europe was moving southwards causing
 245 mainly northerly flow across the alps and at the SBO. Wind speeds observed at the SBO
 246 in the time interval between 1800 and 2000 UTC were between 5 and 10 m s^{-1} (Fig. 4).
 247 In the same time interval temperature decreased by 1 K from -12.5 to -13.5°C . The SBO
 248 was in cloud starting from 1300 UTC with varying visibility between several meters up to
 249 several hundreds of meters. Some snow fall was observed in the afternoon between 1300
 250 and 1500 UTC.

251 For this day wind data of the 3D Sonic Anemometer are available, which allow a
 252 more detailed analysis of the correlation between the observed ICNC and wind speed. Un-
 253 fortunately, only four vertical profiles were obtained with the HoloGondel platform due to
 254 hardware problems with the computer of the platform. The first profile was measured in
 255 the morning at 1200 UTC when the SBO was not in cloud and no ice crystals were ob-
 256 served. Three more profiles were observed in the late afternoon starting from 1800 UTC.
 257 For these profiles the ice crystals have been classified by hand and subclassified in the
 258 three categories: regular, irregular and aggregates.

Figure 8 gives an overview on the three profiles observed in the late afternoon of 17 February. An ICNC of several hundreds was observed in the lowest height intervals with a maximum between 4.1 and 6.0 m. The minimal ICNC was consistently observed for all profiles at 10 m and was always below 150 l^{-1} . The decrease of the ICNC varies between a factor of 2 and 4. In general the observed profiles on this day are similar to the ones observed on 4 February between 2030 and 2200 UTC. This may be explained by very similar meteorological conditions. Wind direction was mainly from North to Northeast and wind speed varied between 5 and 10 m s^{-1} in both measurement intervals. Only temperature was slightly lower on 17 February.

In Figure 9 ICNCs are compared to various wind speeds. In contrast to the data of 4 February no correlation between ICNCs and the horizontal wind speed is observed. This holds true for the one minute average and maximum wind speed of the corresponding time interval observed by the SBO as well as the secondly average observed with the 3D Sonic Anemometer from the HoloGondel Platform. However, Figure 9c shows an increase of ICNC with the vertical wind speed.

All the ice crystals observed on 17 February were classified by hand a subclassification into irregular and regular ice crystals as well as aggregates was realized. The profiles of the subcategorized ICNCs and the relative abundance of these categories on the different heights are shown in Figure 10. ICNCs are dominated by irregular ice crystals, which is in good agreement with various other observations (citations). However, it is surprising to us that the relative importance of the irregular ice crystals stays constant with height or even increases. From surface based ice crystal enhancement processes irregular ice crystals are expected to enhance ICNCs near the surface. With increasing height this influence is expected to decrease and regular ice crystals to become more important. However, from this data a proportional decrease of the absolute number of regular and irregular ice crystals is observed. In Figure 11 the concentration of the different habits is correlated to the vertical wind speed observed. It is clearly visible that the ice crystal number concentration of irregular ice crystals show a stronger dependence on wind speed.

4 Discussion

4.1 Comparison with Nishimura and Nemoto [2005]

Previous studies about the properties of blowing snow focused on the redistribution of snow and its effect on road visibility, avalanche danger as well as mass and energy balance. Therefore, these studies focused on small heights ($<2 \text{ m}$) above flat snow surface (i.e. the saltation and suspension layer). To our knowledge only *Nishimura and Nemoto* [2005] conducted measurements of the properties of blowing snow up to a height of 9.6 m at Mizuho Station, Antarctica. This study will be used for a comparison with our results.

It is known that the particle size distribution at different heights can be well represented with two-parameter gamma probability density functions [*Budd*, 2013; *Schmidt*, 1982]

$$f(d) = \frac{d^{\alpha-1}}{\beta^\alpha \Gamma(\alpha)} \exp\left(-\frac{\beta}{d}\right) \quad (1)$$

with the particle diameter d , the shape parameter α and the scale parameter β . The fitted results for 17 February are shown in Figure 12. The fits show close agreement with the data for all heights. The resulting shape parameter α and the mean diameter, represented by the product of the shape and scale parameter of the gamma-pdf, are plotted in Figure 13. The mean diameter decreases with height and is in the range of 90–110 μm . This is slightly higher than obtained by *Nishimura and Nemoto* [2005], which was in the range of 70–100 μm above a height of 1 m. The shape factor doesn't vary much

306 with height and compares well with values at a height of 1.1-3.1 m from *Nishimura and*
 307 *Nemoto* [2005]. The main differences of the two are, that in this study ICNCs were ob-
 308 served at the top of a mountain in cloud, whereas *Nishimura and Nemoto* [2005] measured
 309 ICNCs above a flat surface in dry air. A larger mean diameter can result from the con-
 310 tribution of cloud ice crystals and the missing sublimation of the ice crystals after lifted
 311 from the surface. A broader gamma-pdf is possibly only a result of the contribution of the
 312 cloud ice crystals to the ICNC. This is supported by the horizontal mass flux calculated
 313 for the data of 17 February (Fig. ??). At a height of 10 m the horizontal mass flux is an
 314 order of magnitude higher than in the study by *Nishimura and Nemoto* [2005].

315 Although a strict comparison between the results of this study with results obtained
 316 by *Nishimura and Nemoto* [2005] is difficult, the discussed agreements are an indication
 317 that the ICNC measurements are strongly influenced by surface-based ice-crystal enhance-
 318 ment processes up to a height of 10 m.

319 **4.2 Wind dependency of the observed ICNCs**

320 The observations on 4 February and 17 February show very different results in re-
 321 spect to a correlation of the ICNCs with wind speed. Whereas the ICNC observed on 4
 322 February shows a clear dependency on horizontal wind speed below 14 m s^{-1} . For higher
 323 wind speeds a possible saturation of the ICNC is reached. For 17 February a dependency
 324 is missing for the observed ICNC on horizontal wind speed. However for the data on 17
 325 February a correlation is observed with vertical wind speed available from the 3D Sonic
 326 Anemometer. Because the vertical wind speed is not available for 17 February possible
 327 reasons for this observation are speculative.

328 Orography? High vertical wind speeds are the driving force on 17 February? Whereas
 329 the high horizontal wind speeds on 4 February are sufficient → Similar horizontal wind
 330 speed on 17 February and 4 February between 20:00 and 22:00 → high vertical wind
 331 speed are a possible reason for the influence at higher heights.

332 In previous literature a wind dependency was observed for ICNCs smaller than 100,
 333 whereas larger ICNCs were wind independent [Lloyd et al., 2015]. Blowing snow, re-
 334 ceptively hoar frost were proposed as the underlying mechanisms for these observations.
 335 Based on our observations we propose that at mountain-top research station not only the
 336 horizontal wind speed may play an important role for the resuspension but also the vertical
 337 wind speed is important → February 17. → observed ice crystal habit on 17 was domi-
 338 nated by irregular ice crystals.

339 In general a correlation with wind speed: difficult to tell, because the time of mea-
 340 surement of a high ICNC and wind speed is not necessarily the time of the suspension
 341 of the ice crystals from the surface, secondly the amount of IC does not only depend on
 342 wind speed, but also on age of the snow cover, temperature. A possible correlation may
 343 be suppressed in a large data set with different snowpack conditions.

344 **4.3 Enhanced concentration of ice crystals with regular habit**

345 **4.4 Implication on atmospheric relevance of mountain-top in-situ measurements**

346 **5 Conclusion**

347 **Acronyms**

348 **SBO** Sonnblick Observatory

349 **Acknowledgments**

350 Sonnbllick Observatory and team (Elke Ludewig, Hermann Scheer, Norbert Daxbacher,
 351 Lug Rasser, Hias Daxbacher)

352 Thanks to Hannes, Olga, Fabiola, Monika, for their help

353 Thanks to Rob for many discussions

354 **References**

- 355 Baumgardner, D., J. Brenguier, A. Bucholtz, H. Coe, P. DeMott, T. Garrett, J. Gayet,
 356 M. Hermann, A. Heymsfield, A. Korolev, M. KrÃdmer, A. Petzold, W. Strapp,
 357 P. Pilewskie, J. Taylor, C. Twohy, M. Wendisch, W. Bachalo, and P. Chuang (2011),
 358 Airborne instruments to measure atmospheric aerosol particles, clouds and radiation:
 359 A cook's tour of mature and emerging technology, *Atmos. Res.*, 102(1â€§2), 10 – 29,
 360 doi:10.1016/j.atmosres.2011.06.021.
- 361 Beck, A., J. Henneberger, S. Schöpfer, J. Fugal, and U. Lohmann (2017), Hologondel, *At-*
 362 *mos. Meas. Tech.*
- 363 Bromwich, D. H. (1988), Snowfall in high southern latitudes, *Reviews of Geophysics*,
 364 26(1), 149–168, doi:10.1029/RG026i001p00149.
- 365 Budd, W. F. (2013), *The Drifting of Nonuniform Snow Particles1*, pp. 59–70, American
 366 Geophysical Union, doi:10.1029/AR009p0059.
- 367 Déry, S. J., and M. K. Yau (1999), A climatology of adverse winter-type weather
 368 events, *Journal of Geophysical Research: Atmospheres*, 104(D14), 16,657–16,672, doi:
 369 10.1029/1999JD900158.
- 370 Farrington, R. J., P. J. Connolly, G. Lloyd, K. N. Bower, M. J. Flynn, M. W. Gallagher,
 371 P. R. Field, C. Dearden, and T. W. Choularton (2015), Comparing model and measured
 372 ice crystal concentrations in orographic clouds during the inupiaq campaign, *Atmos.*
Chem. and Phys., 15(18), 25,647–25,694, doi:10.5194/acpd-15-25647-2015.
- 373 Field, P. R., R. P. Lawson, P. R. A. Brown, G. Lloyd, C. Westbrook, D. Moisseev, A. Mil-
 374 tenberger, A. Nenes, A. Blyth, T. Choularton, P. Connolly, J. Buehl, J. Crosier, Z. Cui,
 375 C. Dearden, P. DeMott, A. Flossmann, A. Heymsfield, Y. Huang, H. Kalesse, Z. A.
 376 Kanji, A. Korolev, A. Kirchgaessner, S. Lasher-Trapp, T. Leisner, G. McFarquhar,
 377 V. Phillips, J. Stith, and S. Sullivan (2017), Secondary ice production: Current state of
 378 the science and recommendations for the future, *Meteorological Monographs*, 58, 7.1–
 379 7.20, doi:10.1175/AMSMONOGRAPH-D-16-0014.1.
- 380 Fugal, J. P. (2017), Holosuite, in preparation.
- 381 Geerts, B., B. Pokharel, and D. a. R. Kristovich (2015), Blowing Snow as a Natural
 382 Glaciogenic Cloud Seeding Mechanism, *Mon. Weather Rev.*, 143(12), 5017–5033, doi:
 383 10.1175/MWR-D-15-0241.1.
- 384 Gultepe, I., G. Isaac, and S. Cober (2001), Ice crystal number concentration versus tem-
 385 perature for climate studies, *International Journal of Climatology*, 21(10), 1281–1302,
 386 doi:10.1002/joc.642.
- 387 Hallet, J., and S. Mossop (1974), Production of secondary ice particles during the riming
 388 process, *Nature*, 249, 26–28, doi:10.1038/249026a0.
- 389 Lachlan-Cope, T., R. Ladkin, J. Turner, and P. Davison (2001), Observations of cloud and
 390 precipitation particles on the avery plateau, antarctic peninsula, *Antarctic Science*, 13(3),
 391 339â€§348, doi:10.1017/S0954102001000475.
- 392 Li, L., and J. W. Pomeroy (1997), Estimates of threshold wind speeds for snow trans-
 393 port using meteorological data, *Journal of Applied Meteorology*, 36(3), 205–213, doi:
 394 10.1175/1520-0450(1997)036<0205:EOTWSF>2.0.CO;2.
- 395 Lloyd, G., T. W. Choularton, K. N. Bower, M. W. Gallagher, P. J. Connolly, M. Flynn,
 396 R. Farrington, J. Crosier, O. Schlenczek, J. Fugal, and J. Henneberger (2015), The ori-
 397 gins of ice crystals measured in mixed-phase clouds at the high-alpine site jungfraujoch,
 398 *Atmos. Chem. Phys.*, 15(22), 12,953–12,969, doi:10.5194/acp-15-12953-2015.

- 400 Lohmann, U. (2002), Possible aerosol effects on ice clouds via contact nucleation, *Journal of the Atmospheric Sciences*, 59(3), 647–656, doi:10.1175/1520-0469(2001)059<0647:PAEOIC>2.0.CO;2.
- 401
402
403 Mahesh, A., R. Eager, J. R. Campbell, and J. D. Spinhirne (2003), Observations of blowing snow at the south pole, *Journal of Geophysical Research: Atmospheres*, 108(D22), n/a–n/a, doi:10.1029/2002JD003327, 4707.
- 404
405
406 Nishimura, K., and M. Nemoto (2005), Blowing snow at mizuho station, antarctica, *Philosophical Transactions of the Royal Society of London A: Mathematical, Physical and Engineering Sciences*, 363(1832), 1647–1662, doi:10.1098/rsta.2005.1599.
- 407
408
409 Palm, S. P., Y. Yang, J. D. Spinhirne, and A. Marshak (2011), Satellite remote sensing of blowing snow properties over antarctica, *Journal of Geophysical Research: Atmospheres*, 116(D16), n/a–n/a, doi:10.1029/2011JD015828, d16123.
- 410
411
412 Rangno, A. L., and P. V. Hobbs (2001), Ice particles in stratiform clouds in the arctic and possible mechanisms for the production of high ice concentrations, *Journal of Geophysical Research: Atmospheres*, 106(D14), 15,065–15,075, doi:10.1029/2000JD900286.
- 413
414
415 Rogers, D. C., and G. Vali (1987), Ice crystal production by mountain surfaces, *J. Clim. Appl. Meteorol.*, 26(9), 1152–1168, doi:10.1175/1520-0450(1987)026<1152:ICPBMS>2.0.CO;2.
- 416
417
418 Rotunno, R., and R. A. Houze (2007), Lessons on orographic precipitation from the mesoscale alpine programme, *Quarterly Journal of the Royal Meteorological Society*, 133(625), 811–830, doi:10.1002/qj.67.
- 419
420
421 Schlenzeck, O., and J. Fugal (2017), Microphysical properties of ice crystal precipitation and surface-generated ice crystals in a high alpine environment in switzerland, *esult*, 56, 433–453, doi:10.1175/JAMC-D-16-0060.1.
- 422
423
424 Schmidt, R. A. (1982), Vertical profiles of wind speed, snow concentration, and humidity in blowing snow, *Boundary-Layer Meteorology*, 23(2), 223–246, doi:10.1007/BF00123299.
- 425
426
427 Vali, G., D. Leon, and J. R. Snider (2012), Ground-layer snow clouds, *Quarterly Journal of the Royal Meteorological Society*, 138(667), 1507–1525, doi:10.1002/qj.1882.
- 428
429 Vionnet, V., G. GuyomarcâŽh, F. N. Bouvet, E. Martin, Y. Durand, H. Bellot, C. Bel, and P. PugliaÃlse (2013), Occurrence of blowing snow events at an alpine site over a 10-year period: Observations and modelling, *Advances in Water Resources*, 55, 53 – 63, doi:<http://doi.org/10.1016/j.advwatres.2012.05.004>, snowâŠAtmosphere Interactions and Hydrological Consequences.
- 430
431
432 Yang, J., and M. K. Yau (2008), A new triple-moment blowing snow model, *Boundary-Layer Meteorology*, 126(1), 137–155, doi:10.1007/s10546-007-9215-49.
- 433
434
435

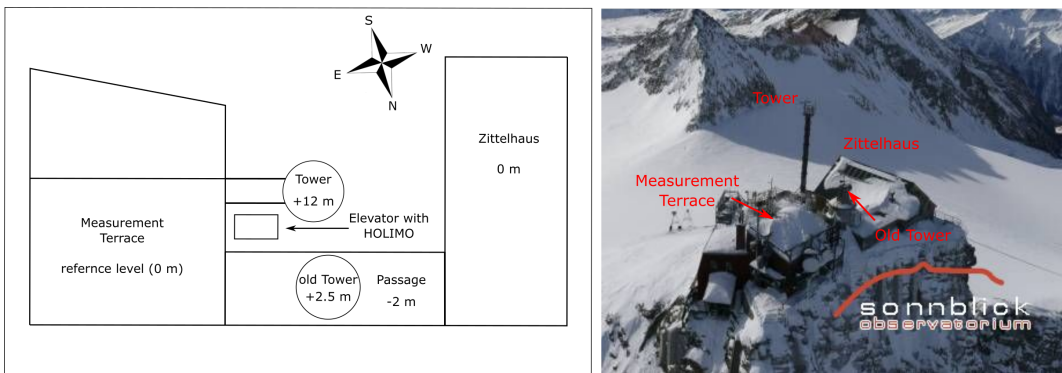


Figure 1. Sketch of the experimental setup and the surrounding structures (left) with their heights relative to the bottom of the measurement terrace. Aerial image of the Sonnblick Observatory (right).

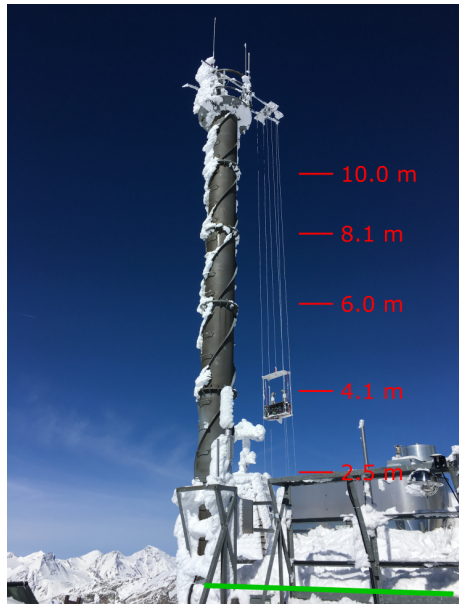
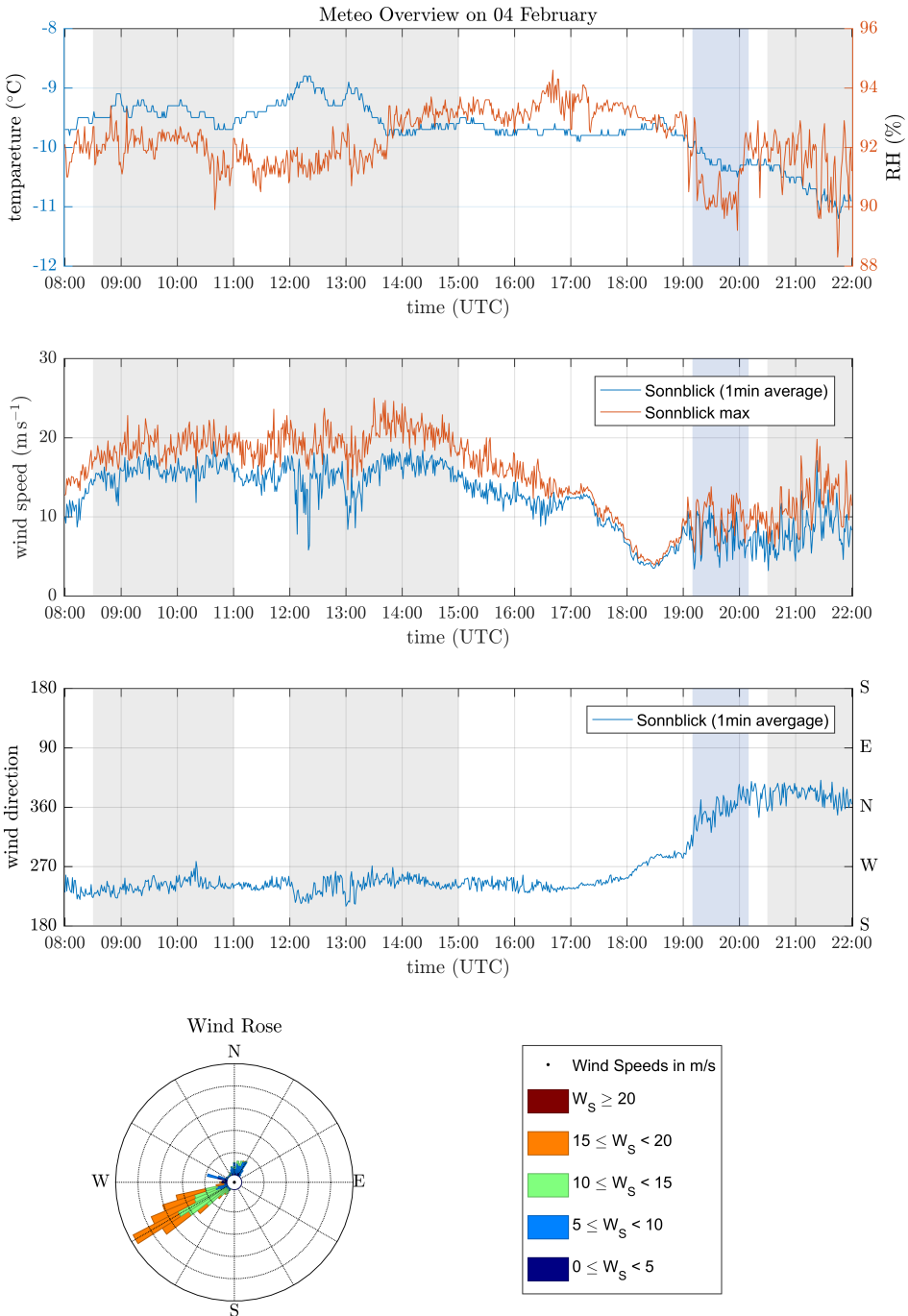
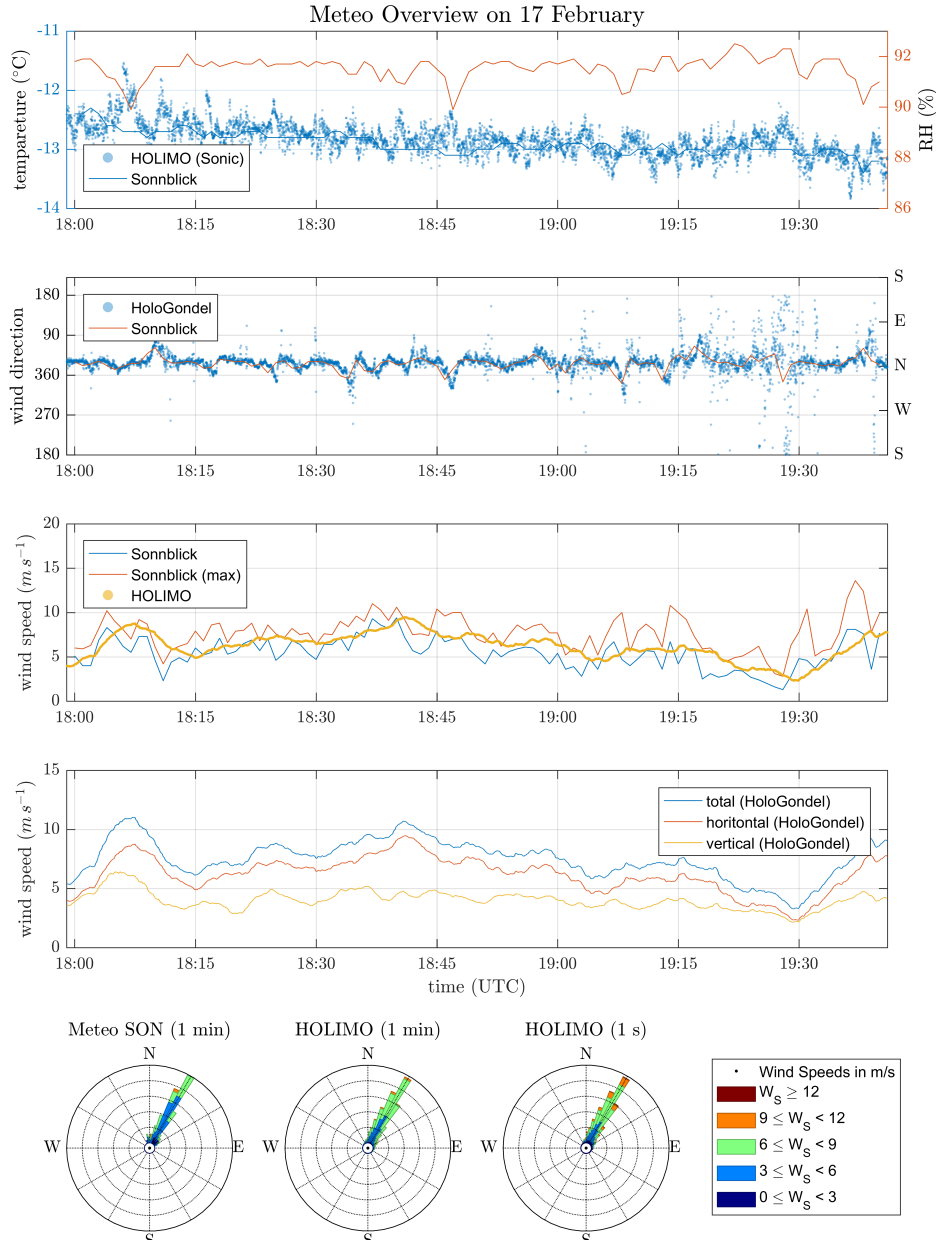


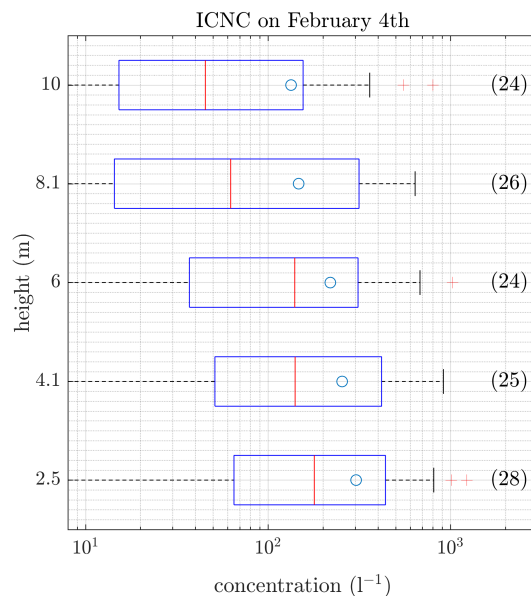
Figure 2. Set up of the elevator with the holographic imager HOLIMO mounted to the meteorological tower at the SBO. The red lines and numbers indicate the five different heights where the elevator was positioned repeatedly to obtain vertical profiles of the ICNC. The reference height of 0.0 m is the bottom of the measurement platform (green line).



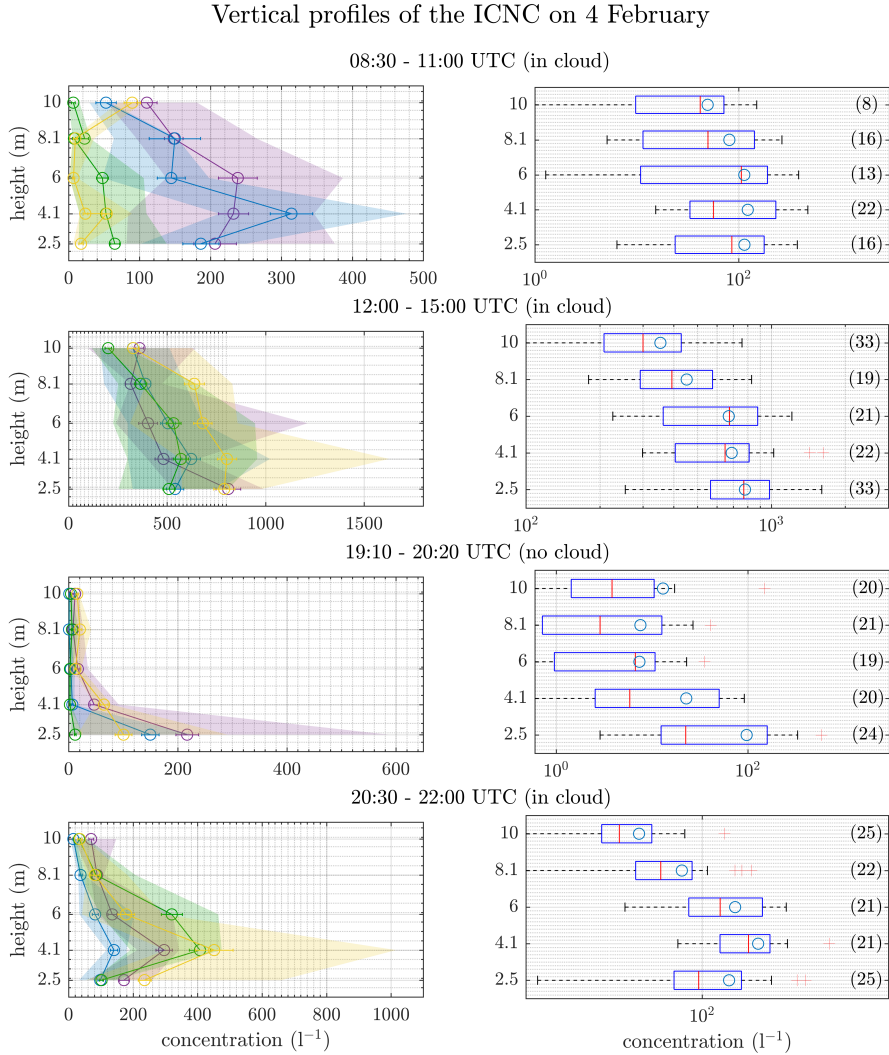
442 **Figure 3.** Overview of the meteorological conditions on 4 February obtained from the SBO measurements.
443 Shown are the temperature, relative humidity (top), wind speed (second from top) and wind direction (second
444 from bottom). All measurements are 1 min averages except for the maximum wind speed, which corresponds
445 to the maximum wind speed observed during a corresponding 1 min average. Grey and blue shaded areas
446 represent time with measurement (see Fig. 6) when the SBO was in cloud, respectively not in cloud. A wind
447 rose plot (bottom) of the wind measurement is also shown.



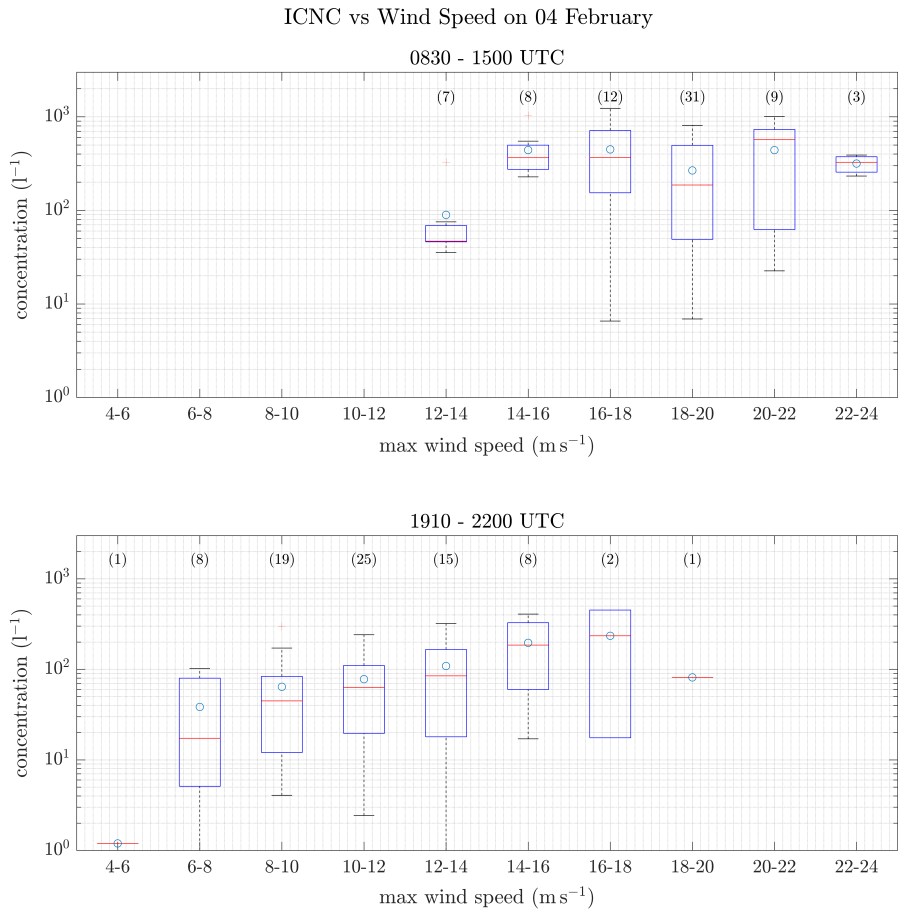
448 **Figure 4.** Overview on the meteorological conditions on 17 February for the time interval when measure-
 449 ments exist (see Fig. 8). On this day temperature and wind measurements are available from the SBO and the
 450 3D Sonic Anemometer. Shown are the temperature and relative humidity (top), wind direction (second from
 451 top), a comparison of the horizontal wind speed (middle) and detailed wind speed measurements from the 3D
 452 Sonic Anemometer (second from bottom). A windrose plot is shown in the bottom panel.



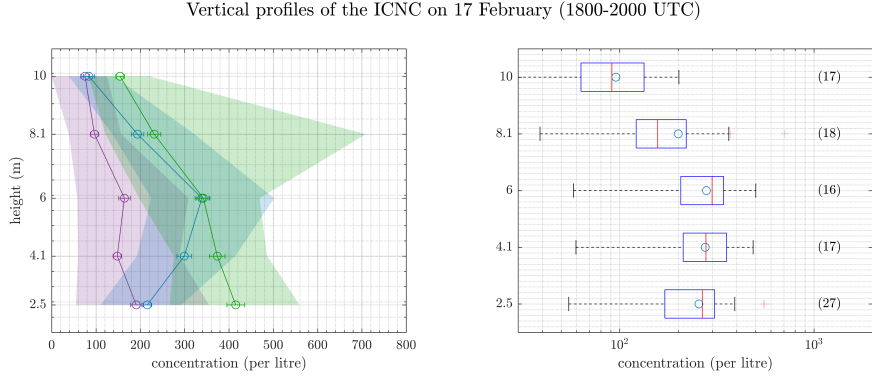
453 **Figure 5.** ICNC as a function of the height of the elevator at the meteorological tower of the SBO. This plot
 454 is a summary of the 24 profiles obtained on 4 February. The data was averaged over the entire time period
 455 of single measurements at the different height. The number in brackets is the number of concentration
 456 measurements per height. For each box, the central line marks the median value of the measurement and the
 457 left and right edges of the box represent 25th and the 75th percentiles respectively. The whiskers extend to
 458 minimum and maximum of the data; outliers are marked as red pluses. The mean value of the measurements
 459 is indicated as a blue circle.



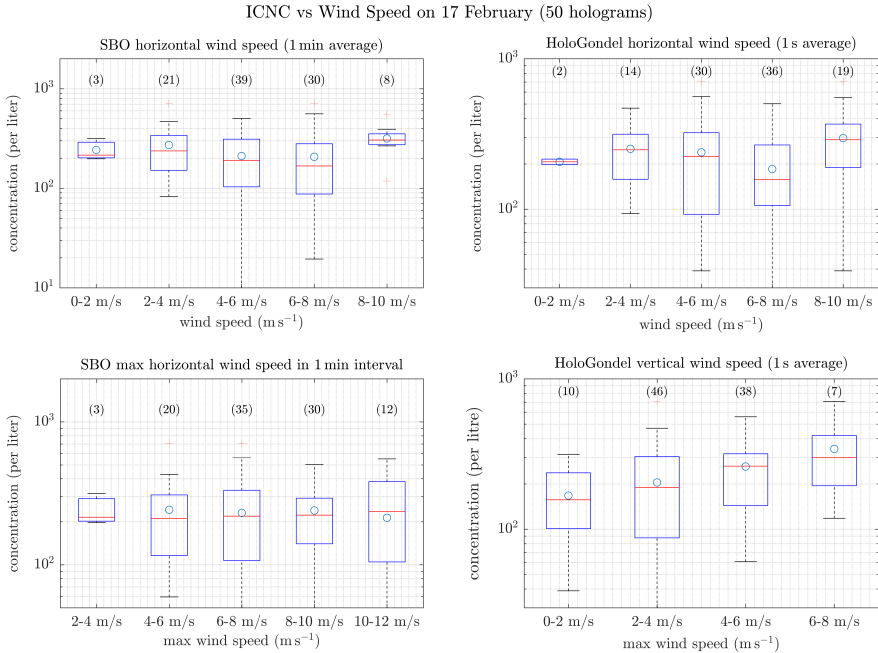
460 **Figure 6.** ICNCs as a function of height of the elevator for four different time intervals during 4 February,
461 representing different conditions (Fig. 3). On the individual profiles (left), the circles indicate the mean value
462 averaged over the entire time interval. The error bars represent the standard error of the mean. The shaded
463 area extends from the minimum to the maximum of the measured ICNC. As in Fig. 5 only for the four time
464 intervals the box plots (right) show a summary of the data.



465 **Figure 7.** As Figure 5 only ICNC as a function of horizontal wind speed for the the time periods between
 466 0830 and 1500 UTC when the wind direction was West-Southwest (top) and between 1910 and 2200 UTC
 467 when the wind direction was North (bottom). The wind speed is the maximum wind speed in one minute time
 468 intervals from the SBO.



469 **Figure 8.** Ice crystal number concentration as a function of the height of the elevator at the meteorological
 470 tower of the SBO for 17 February. On the left are the three individual profiles obtained in cloud. The circles
 471 indicate the mean value averaged over the entire time interval. The error bars represent the standard error of
 472 the mean. The shaded area indicates the variability of the data and extends from the minimum to the maxi-
 473 mum when the data is averaged over 50 holograms. For the summary of the different time intervals (right) the
 474 data is averaged over 50 holograms. For each box, the central line marks the median value of the measurement
 475 and the left and right edges of the box represent 25th and the 75th percentiles respectively. The whiskers
 476 extend to minimum and maximum of the data; outliers are marked as red pluses.



477 **Figure 9.** As Figure 7 only for 17 February and four different wind speed measurements: a) one minute
 478 averages of the horizontal wind speed from the SBO, b) maximum wind speed of the a corresponding time
 479 interval in a), c) secondly averages of the horizontal wind speed and d) secondly average of the vertical wind
 480 speed both from the 3D Sonic Anemometer.

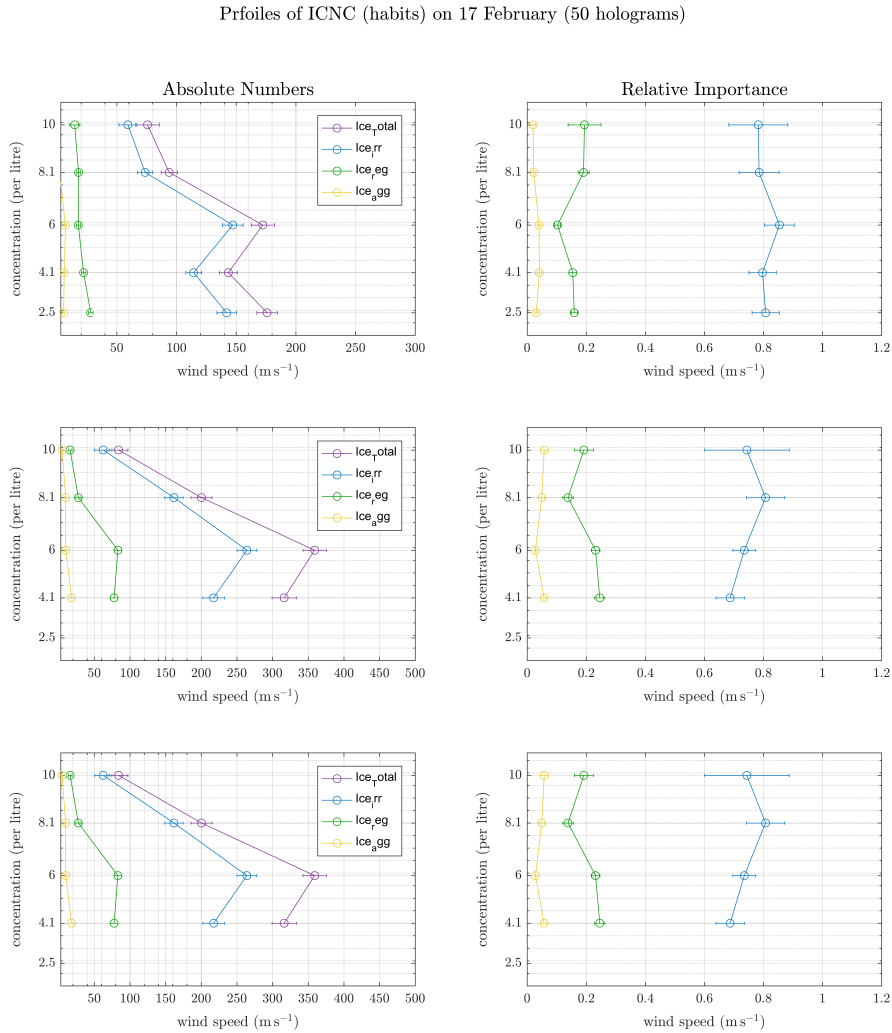
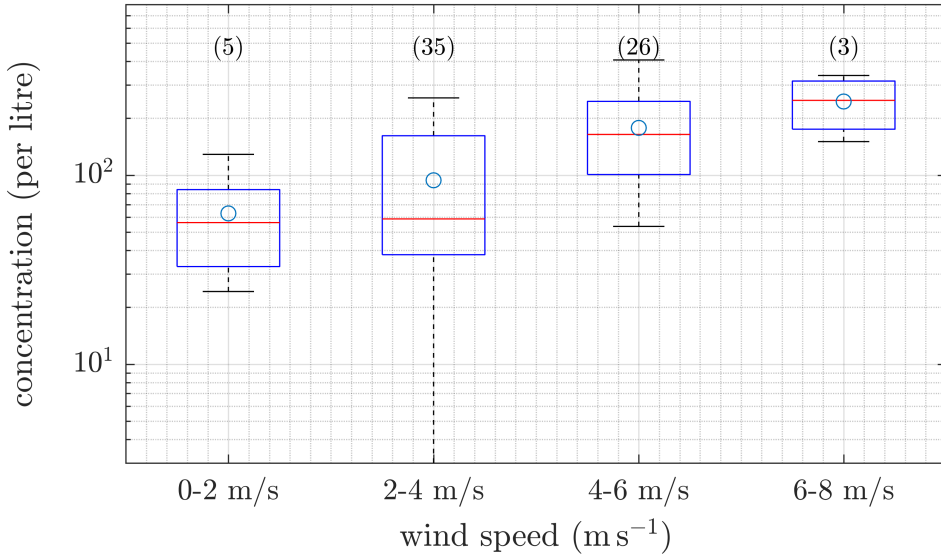


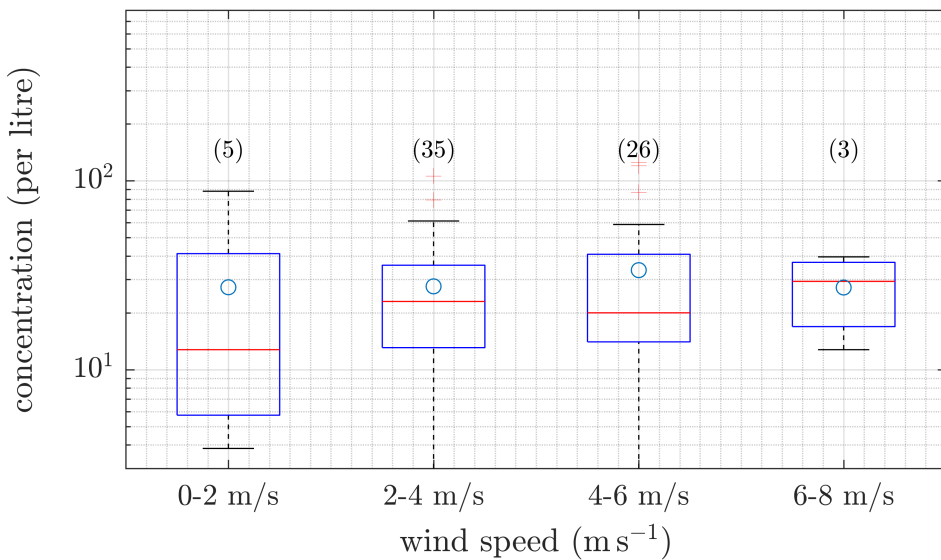
Figure 10. Vertical profiles of the concentration (left) and the relative importance (right) of the subclassified ice crystal habits: regular, irregular and aggregates. For the relative importance the number of ice crystals of different habits were divided by the total number of ice crystals. For theses plots the data as averaged over 50 holograms. In both cases the circles represent the mean of the 50 hologram averages. The error bars represent the standard error of the mean.

ICNC (habits) vs Wind Speed on 17 February (50 holograms)

Irregular Ice Crystals

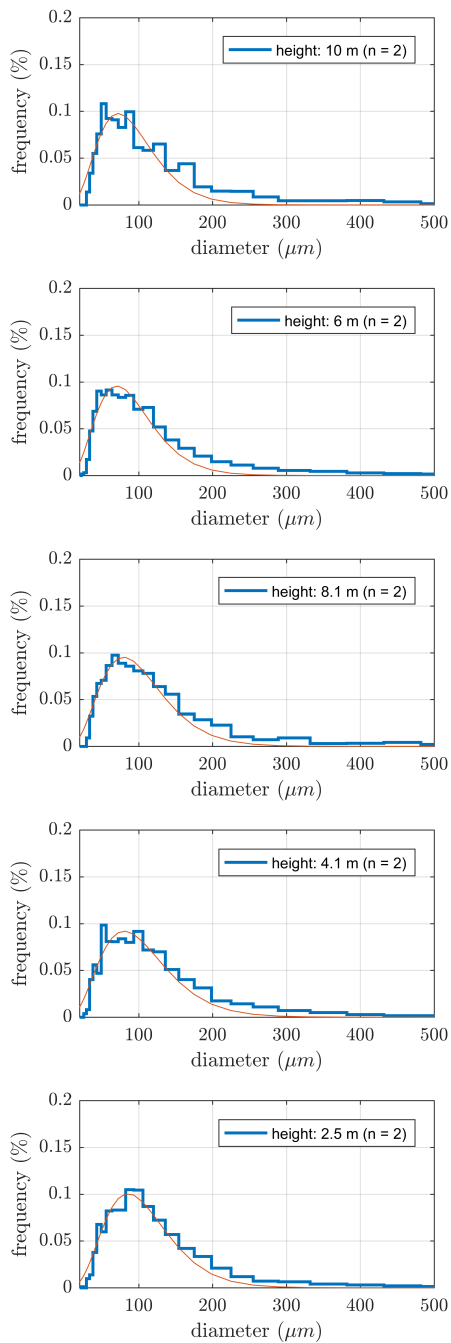


Regular Ice Crystals

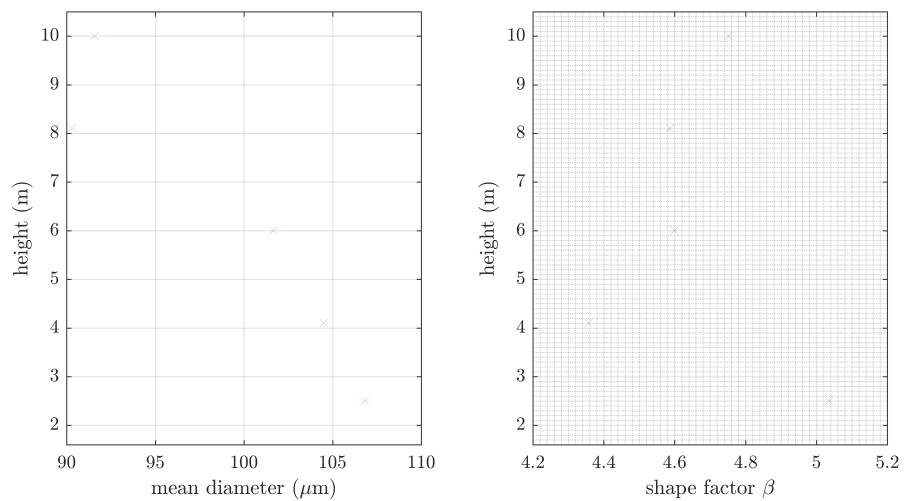


486
487

Figure 11. As Figure 7 only for 17 February and different ice crystal habits as a function of the vertical wind speed.



488 **Figure 12.** As Figure 7 only for 17 February and different ice crystal habits as a function of the vertical
 489 wind speed.



490 **Figure 13.** As Figure 7 only for 17 February and different ice crystal habits as a function of the vertical
491 wind speed.